ABUAD Journal of Engineering Research and Development (AJERD)
ISSN (online): 2645-2685; ISSN (print): 2756-6811

Volume 8, Issue 1, 215-225

Thermodynamics and Adsorption of Fe^{2+} from Oilfield Produced Water using Clay-derived Zeolite

Kingsley Ifeanyi OSUALA[1], Akindele Oyetunde OKEWALE[2]

[1]*Gas and Utilities Company Limited, Port Harcourt, Nigeria*
osuala.kingsley@yahoo.com

[2]*Department of Chemical Engineering, Federal University of Petroleum Resources, Effurun, Delta State, Nigeria*
okewale.akindele@fupre.edu.ng

Corresponding Author: osuala.kingsley@yahoo.com, *+234 09062887417*
Date Submitted: *20/01/2025*
Date Accepted: *06/04/2025*
Date Published: *07/04/2025*

Abstract: *The study explored the potential of clay-derived zeolite (CDZ) as an adsorbent for the removal of Fe^{2+} ions from produced water generated from oil fields. The clay was sourced from the Ikepshi Community in the Akoko-Edo Local Government Area of Edo State, Nigeria. The zeolite was produced through a calcination process at a temperature of 600 °C, followed by dealumination and zeolite synthesis prior to its application for adsorption of Fe^{2+} from produced water. A variety of operational parameters were evaluated to understand their impacts on the adsorption process. These included different dosages of the adsorbent, contact time, temperature, agitation speed, and pH levels. The thermodynamics parameters were evaluated over a temperature range of 303 K to 343 K. Scanning Electron Microscopy (SEM) images displayed the characteristic silicate flakes of kaolinite clay, while Fourier Transform Infrared Spectroscopy (FTIR) results identified specific functional groups. Particularly, the presence of O-H and Si-O stretching vibrations confirmed the clay kaolinite composition. The analysis of adsorption outcomes across varying temperatures revealed negative values for Gibbs free energy (ΔG), and a positive entropy value (ΔS^o), this indicates that the adsorption process is spontaneous and feasible, along with an increase in degree of randomness of adsorption process. The process of Fe^{2+} uptake on CDZ was considered as endothermic, as shown by the positive enthalpy values (ΔH) obtained thus shows a strong Vander Waal forces between the adsorbent and adsorbate.*

Keywords: *Thermodynamics, Clay-derived Zeolite, Adsorption, Oilfield Produced Water*

1. INTRODUCTION

Oilfield-produced water comprises of various organic and inorganic components. Information on the volume and characteristics of the effluent discharge can only be accessed by the operating companies and regulatory agencies. Discharged produced water can contaminate the surface, underground water, and soil. The results of discharging produced water on the environment have been a source of serious environmental concern [1]. The maximum discharge limit of Fe^{2+} ions in produced water has been reported according to the Nigerian Midstream and Downstream Petroleum Regulatory Authority (NMDRPA) standard to be 1.0 mg/L [2]. An elevated presence of Fe^{2+} ions in human body can lead to significant harm including the risk of poisoning. If this discharge limit is exceeded, it can cause blockage, pipeline corrosion, and environmental and biological hazards to the aquatic lives and animals. Therefore, there is a need to reduce the content of Fe^{2+} ions in produced water to a concentration that is less than 1.0 mg/L prior to its discharge. Adsorption has been considered as one of the efficient techniques for the treatment of heavy metals present in wastewater. This technique is promising and has several advantages over others, which justifies its application in the treatment of produced water. One of the great advantages of this technique is its versatility, due to the use of several materials as adsorbents from activated carbon to industrial wastes [3].

The principle of adsorption depends on whether the solid surface that comes into contact with liquids tends to accumulate on surface layer of solute molecules due to the imbalance of existing surface forces, increasing the need for adsorbents that can provide complex and effective abilities for these metal ions [4].

Clay-derived zeolite (CDZ) has many advantages over other existing technologies. Besides having excellent adsorption ability, they are economical and can be retrieved from natural compounds.

They are naturally occurring aluminosilicate minerals that have large capacities for cation exchange, they are less expensive, and provide significant benefits in the removal of metallic ions [5]. The efficiency of the adsorption process using CDZ is influenced by several parameters such as pH levels, adsorbent dosage, temperature, pressure, contact time, surface area, and coexisting ions [6]. Thermodynamics plays a significant role in adsorption processes [7, 8]. Enthalpy measures the heat change during adsorption [9]. For physical adsorption, the process is usually exothermic (releases heat), indicating weak Vander Waal forces [10]. In contrast, chemisorption can be either exothermic or endothermic (absorbs

heat) due to the formation of chemical bonds [11]. Entropy assesses the disorder or randomness in the system [12]. During adsorption, the entropy usually decreases as the adsorbate molecules move from a gaseous or liquid state to a solid surface, becoming more ordered [13,14]. Gibb's free energy determines the spontaneity of the adsorption process [15,16]. A negative ΔG indicates a spontaneous adsorption process, where the magnitude and sign depend on enthalpy and entropy changes [17].

This study is focused on the removal of Fe^{2+} ions from oil-field produced water by utilizing CDZ as adsorbent material under different operational parameters such as adsorbent dosage, contact time, temperature, agitation speed and pH levels in order to understand their impacts on the adsorption process. The thermodynamics parameters, including enthalpy, entropy, and Gibbs free energy were studied, and the removal efficiency of Fe^{2+} ions from produced water was also determined.

2. MATERIALS AND METHODS

2.1 Materials

The clay sample used for the production of zeolite was obtained from a natural clay deposit in Ikepshi Community, Akoko- Edo Local Government Area, Edo State, Nigeria. The oil field produced water sample used in this study was collected from a three-phase Low- Pressure Separator in a Flow Station within Niger – Delta region. Handheld digital pH meter (pH818 Smart sensor instrument, Mainland, China), UV-Vis spectrophotometer (Spectrum lab 755s), Orbital incubator (HY-4A Cycling Vibrator, PEC Medicals USA), Electric muffle furnace (SSI-049), Magnetic stirrer, Autoclave (70706A-MJG18L1_SST), conical flasks, bakers, mesh and digital weighing balance (WT6002K) were employed in this work. Sulphuric acid, sodium hydroxide solutions used were of analytical grades (Sigma Aldrich) and were procured from a qualified chemical dealer in Effurun, Delta State, Nigeria. Distilled water was obtained from Chemical Engineering Laboratory, Federal University of Petroleum Resources, Effurun, Delta State, Nigeria for sample preparation and solutions.

2.2 Sample Preparation and Characterization

The clay sample was cleaned of every debris and unwanted materials prior to its use for the investigation. The beneficiated clay was converted to metakaolin and then leached with sulphuric acid to achieve the required silica-alumina ratio for zeolite synthesis. The beneficiation was done using the method of [18]. The kaolin powder was oven –dried at 120 ℃ for 14 hours. This caused decomposition leading to the destruction of the structure and removal of unwanted volatile components that resulted to metakaolin clay. Sulphuric acid was employed as the leaching agent due to its ability to dissolve and extract zeolites effectively. The leaching process was conducted at 60 ℃ for 3 hours while maintaining a stirring speed of 300 rpm to achieve the silica-alumina for the zeolite synthesis. The adsorbent was activated using the method of [19]. The clay sample was calcined in a muffle furnace at a temperature of 600 ℃ for 2 hours. Thereafter, the calcined clay samples were cooled to room temperature, the dried clay sample was activated with both 0.5 M of H_2SO_4 and NaOH in the ratio 1:1 clay (acid/ base) for 24 hours. This is to produce a clay of high surface area and high degree of micro-porosity.

2.3 Dealumination of Clay

In order to adjust the mole ratio of Si/Al, 200 g of calcined clay was dealuminated by mixing 500 mL of 60 wt% H_2SO_4 solution in a 1000 mL round bottom flask and stirred to form a homogeneous mixture with the aid of a magnetic stirrer and left to react without external heating for about 10 minutes, thereafter, it was heated at 120 ℃ for 25 minutes. The temperature of the reaction was noted to start from 55 ^oC and progressed to 120 ^oC [20]. The reaction was stopped, and the collected dealuminated clay sample was washed with deionized water until a neutral pH was achieved, filtered, oven dried at 120 ^oC for 4 hours, and stored in a desiccator for further laboratory analysis.

2.4 Synthesis of Zeolite from Dealuminated Clay

1000 mL of 5.0 M NaOH solution was prepared and gradually added to specific mass of calcined clay to obtain an aluminosilicate gel in accordance with the method of [21]. The gel was continuously stirred at room temperature for 120 minutes with a magnetic stirrer and allowed to age for 24 hours. A hydrothermal treatment was performed on the mixture at 120 ^oC for 6 hours with the aid of an autoclave, after which the mixture was subjected to drying in the oven for 4 hours at 105 ^oC to remove any inherent moisture content.

2.5 Adsorbate Characterization

The produced water sample was analyzed for heavy metals concentration such as Cu^{2+}, Pb^{2+}, Fe^{2+}, Zn^{2+}, and Cr^{3+} ions using UV-Vis spectrophotometer. Other parameters of the produced water such as pH, temperature and conductivity were also characterized in accordance with established guidelines and procedures according to [22] using multiparameter probe.

2.6 Fourier Transform Infra Ray Spectroscopy (FTIR)

The structural organization of the clay sample was investigated to detect the functional groups present. The sample was examined using a buck scientific infrared spectrophotometer (4500a) with a range 500 – 4000 cm^{-1} (wavelength). KBr (potassium bromate) was used as a background material in the analysis. The result of FTIR analysis on the sample gave valuable information about its chemical functional group composition and structural properties.

2.7 Scanning Electron Microscope (SEM)

The surface condition of both the raw clay and CDZ samples were analyzed with the aid of a 52-cm scanning electron microscope (SEM) JSM- IT810 at a magnification of 100 µm and 10 µm. A concentrated electron beam was used to scan the sample with an electron microscope to obtain images of the sample. The samples atoms and electrons interact, resulting in a variety of detectable signals that revealed details about the sample surface morphology and composition.

2.8 Batch Adsorption Experimental Procedure

The batch adsorption experiment was carried out using produced water as adsorbate with the method described by [23]. Different adsorbent dosages of 0.2, 0.4, 0.6, 0.8 and 1.0 g were placed in 250 mL conical flasks containing 50 mL of produced water which were agitated for time intervals of 20, 30, 40, 50 and 60 minutes using orbital shaker at different agitation speed of 100, 120, 140, 160 and 200 rpm, temperature intervals of 30, 40, 50, 60 and 70 ℃ and pH intervals of 2, 4, 6 and 8. Thereafter, the samples were filtered using Whatman filter paper. The supernatants were filtered and analyzed for Fe^{2+} ions concentration using UV-visible Spectrophotometer (spectrum lab 755s) at 248.3 nm wavelength.
The amount of equilibrium adsorption, q_e (mg g^{-1}) was calculated using equation (1) while the percentage adsorption was calculated using equation (2). The process was repeated to study the effect of time, temperature, agitation speed and adsorbent dosage.

$$\mathrm{qe} = \frac{(\mathrm{Co}-\mathrm{Ce})}{\mathrm{m}} V \quad (1)$$

Percentage removal was also calculated according to the equation below

$$\%\ \text{Removal or adsorption} = \frac{(\mathrm{Co}-\mathrm{Ce})}{\mathrm{Co}} \times 100 \quad (2)$$

Where, C_o and C_e (mg L^{-1}) are the initial and equilibrium concentrations of Fe^{2+} ions respectively. V is the volume of the solution (mL) and m is the mass of the adsorbent used in (g).

1. Effect of CDZ Dosage: To evaluate the effect of adsorbent dosage on the adsorption capacity and percentage sorption of Fe^{2+}, varying amounts of CDZ (0.2g, 0.4g, 0.6g, 0.8g, and 1.0g) were tested. Each set was observed at 30 minutes, while maintaining a constant pH of 7.0 and temperature of 25°C.
2. Effect of Temperature: The impact of temperature on Fe^{2+} adsorption was examined at temperatures of 30°C, 40°C, 50°C, 60°C, and 70°C using a cyclic water bath set to an agitation speed of 200 rpm for 60 minutes. Different dosages of zeolite adsorbent (0.2g, 0.4g, 0.6g, 0.8g, and 1.0g) were added to conical flasks containing 50 mL of produced water. The pH of the produced water was maintained at 7.0.
3. Effect of Contact Time: To study the effect of contact time, 250 mL conical flasks containing 50 mL of produced water were prepared, each with varying amounts of zeolite adsorbent (0.2g, 0.4g, 0.6g, 0.8g, and 1.0g) derived from clay. The pH of the produced water was adjusted to 7.0, and the mixtures were agitated at 200 rpm using an orbital shaker for different time intervals: 20, 30, 40, 50, and 60 minutes. The treated water was then filtered using Whatman No. 1 filter paper, and Fe^{2+} concentrations were measured with a UV-visible spectrophotometer at a wavelength of 248.3 nm. The study was carried out at 25°C.
4. Effect of Agitation Speed: The influence of agitation speed on adsorption capacity and Fe^{2+} removal efficiency was analyzed using different shaking speeds: 100 rpm, 120 rpm, 140 rpm, 160 rpm, and 200 rpm. An orbital incubator shaker was used to agitate the samples in a circular motion. The concentration of Fe^{2+} adsorbed from the produced water was determined. The experiment was conducted at a constant temperature of 25°C, pH of 7.0 for 60 minutes, with adsorbent dosages of 0.2g, 0.4g, 0.6g, 0.8g, and 1.0g.
5. Effect of pH: The pH of the samples was adjusted to 2, 4, 6, and 8 using 1M NaOH. Five conical flasks, each containing 50 mL of produced water, were prepared. Different amounts of zeolite (adsorbent) — 0.2g, 0.4g, 0.6g, 0.8g, and 1.0g — were added to each flask, and the effect of pH on adsorption was studied at the selected pH levels. The mixtures were intermittently stirred for 30 minutes and then agitated at 200 rpm using a rotary shaker for 60 minutes to achieve equilibrium. After treatment, the samples were filtered using Whatman No. 1 filter paper, and Fe^{2+} concentrations were determined using a UV-visible spectrophotometer at a wavelength of 248.3 nm. The experiment was conducted at 25°C. To prevent fluctuations in pH due to gas exchange, the conical flasks were properly sealed.

3. RESULTS AND DISCUSSION

3.1 Characterization of Oil field Produced Water

Table 1 shows the laboratory analysis performed on oil field produced water to determine the preponderance of heavy metals composition and other parameters. The concentration of Fe^{2+} ions was found to be 1.259 mg/L, which is above the disposable limit for effluent water discharge in Nigeria (NMDPRA standard) shown in Table 1 as reported by [24].

3.2 Fourier Transform Infrared Spectroscopy (FTIR)

Figures 1 and 2 illustrate the FTIR spectra of the raw clay and CDZ samples, respectively, highlighting the specific functional groups present. In Figure 1, the wavenumber at 3369.5 cm^{-1} corresponds to the O–H bond, indicate hydroxyl

groups. These groups enhance the clay ability to interact with the produced water through physisorption or chemisorption [25]. The broad band at 2322.1 cm^{-1} suggests the presence of O=C=O stretching, expectedly due to adsorbed CO_2, which can be attributed to the clay high surface area and adsorption capacity.

Table 1: Laboratory analysis of produced water

Parameters	Produce Water Sample	NMDPRA limit
pH	8.17	6.5-8.5
Temperature, ^{O}C	26.7	25
Conductivity, µs/cm	1129	-
Iron (Fe), mg/L	1.259	1.0
Chromium (Cr), mg/L	0.429	0
Zinc (Zn), mg/L	0.512	1.0
Copper (Cu), mg/L	0.446	1.0
Lead (Pb), mg/L	0.098	0.05

A broad band at 2166.6 cm^{-1} in Figure 1 corresponds to alkyne stretching vibrations, typically appearing between 2100–2260 cm^{-1}. This shows the presence of organic material with triple bonds, supporting the clay adsorption potential.

Figure 2 depicts the CDZ sample which exhibits a wavenumber of 2176.8 cm^{-1}, suggests the functional group containing alkyne organic compounds. The peak at 2031.4 cm^{-1} in Figure 1 corresponds to M–CO stretching vibrations (typically found between 1800–2100 cm^{-1}), indicating the presence of metal-containing compounds with CO ligands. Similarly, the wavenumber at 2013.4 cm^{-1} in Figure 2 suggests the formation of metal carbonyl complexes, providing evidence of modification during zeolite preparation. The existence of peak with wavenumber at 1051.1 cm^{-1} in Figure 1 corresponds to Si–O stretching vibrations, characteristic of silicate minerals. These vibrations demonstrate the silicate framework, which plays a crucial role in the clay ability to adsorb cations and water. In Figure 2, a peak at 1040.0 cm^{-1} confirms the successful transformation of clay minerals into a zeolite framework [26].

Additionally, the existence of peak at 1643.8 cm^{-1} in Figure 1 corresponds to bending vibrations of adsorbed water molecules, as bands near 1640–1645 cm^{-1} are typically associated with water adsorption. Peaks in the 600–900 cm^{-1} range often indicate bending vibrations in aromatic compounds [27]. Specifically, the peak at 775.3 cm^{-1} in Figure 1 suggests C–H out-of-plane bending in aromatic rings, confirming the presence of organic matter in the clay sample. In Figure 2, the peaks at 670.9 cm^{-1} and 798 cm^{-1} within this range indicate the formation of zeolite after the transformation from clay.

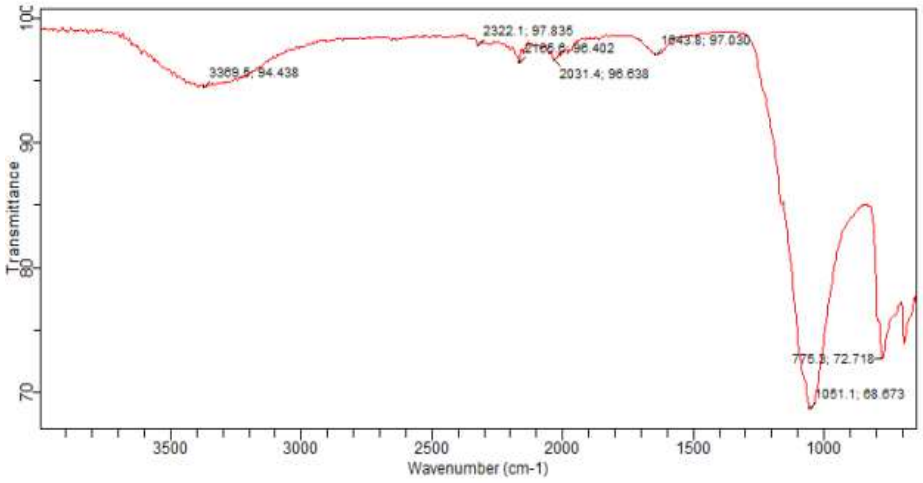

Figure 1: The result of FTIR of the raw clay sample

Table 2: Wavenumber and the intensity of raw clay sample as captured by FTIR

Peak Number	Wavenumber(cm^{-1})	Intensity (%)
1	1051.1	68.673
2	775.3	72.718
3	1643.8	97.030
4	2031.4	96.638
5	2166.6	96.402
6	2322.1	97.835
7	3369.5	94.438

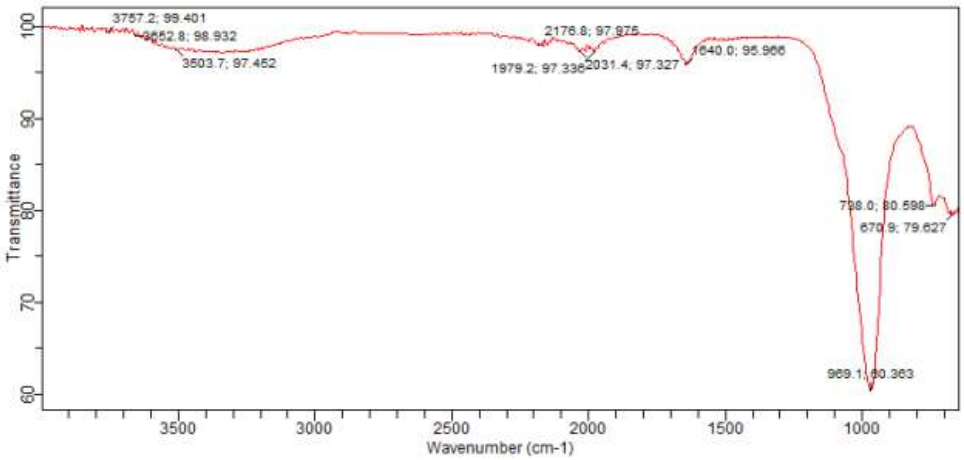

Figure 2: The result of FTIR of clay-derived zeolite sample

Table 3: Wavenumber and the intensity of Zeolite sample as captured by FTIR

Peak Number	Wavenumber (cm^{-1})	Intensity %
1	670.9	79.627
2	798.0	80.598
3	969.1	60.363
4	1040.0	95.900
5	2013.4	97.327
6	2176.8	97.975
7	3503.7	97.452
8	3652.8	98.932
9	3652.8	98.32
10	3757.2	99.401

3.3 Scanning Electron Microscopy (SEM)

Images taken from SEM display the silicate flakes of kaolinite clay which is similar to the work done by [28]. The raw clay sample image was shown in figure 3a, image of CDZ sample (figure 3b) and image of spent CDZ sample (figure 3c) respectively. SEM image of figure 3b, zeolite before adsorption reveals the porous nature of the zeolite structure, showcasing the size, shape, and distribution of pores. A higher surface area and well-distributed pores facilitate better contact with adsorbates, enhancing the adsorption capacity. SEM image of figure (3c), CDZ image after adsorption reveals several morphological changes which include that the pores within the zeolite framework has become partially saturated with adsorbate, the zeolite also exhibit rough surface texture post -adsorption and changes in morphology that resulted in modification of effective surface area. By examining the raw clay, adsorbent and spent adsorbent at high magnification, its texture, distribution of active sites, and potential sites of adsorption can be assessed [29].

(a) (b) (c)

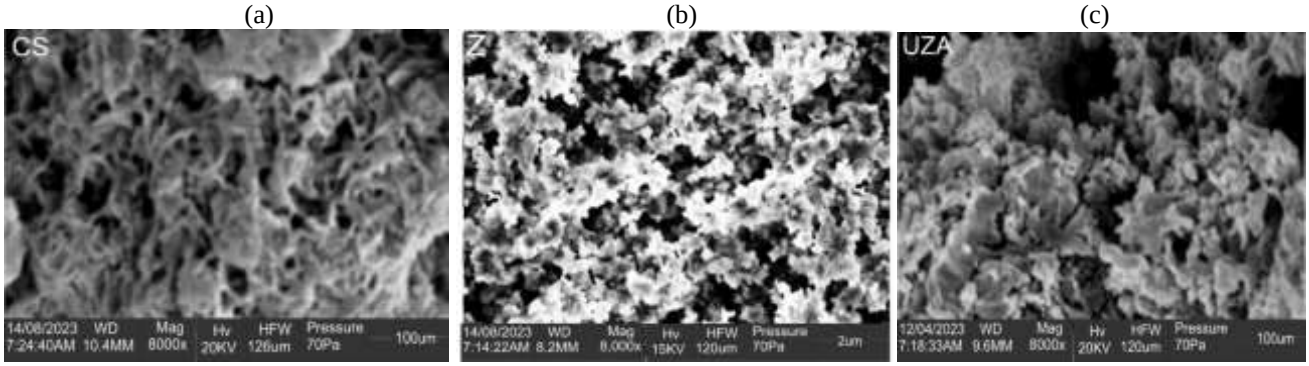

Figure 3: SEM images of (a) Raw Clay (b) CDZ before adsorption (c) CDZ after adsorption

3.4 Batch Adsorption

The effects of various operational parameters, including adsorbent dosage, contact time, temperature, agitation speed, and pH level, were evaluated using the batch adsorption method to determine the optimum conditions for Fe^{2+} removal. Figure 4(a) demonstrates that Fe^{2+} adsorption increases progressively with higher adsorbent dosage. This trend is attributed to the greater availability of adsorption sites and increased surface area for Fe^{2+} uptake from produced water [30]. The maximum adsorption was observed at 52.45 % with a 1.0 g adsorbent dosage.

Similarly, Figure 4(b) illustrates the effect of temperature on Fe^{2+} removal, it shows that adsorption efficiency improves with increasing temperature. This can be explained by the enhanced mobility of Fe^{2+} ions at higher temperatures [31], as well as possible swelling of the adsorbent internal structure, which facilitates greater Fe^{2+} penetration. Additionally, higher temperatures may lead to pore enlargement and activation of the sorbent surface, further enhancing adsorption [32]. The highest adsorption efficiency was recorded at 52.58 % at 70 °C.

Contact time is another critical factor in the adsorption process, as shown in Figure 4(c). The adsorption of Fe^{2+} by CDZ increases with time until equilibrium is reached. The maximum Fe^{2+} adsorption efficiency of 52.45 % occurred at 60 minutes, beyond which no further Fe^{2+} uptake was observed, indicating equilibrium conditions.

The effect of agitation speed on Fe^{2+} removal is depicted in Figure 4(d). The uptake of Fe^{2+} increased significantly at 100 rpm and 120 rpm, with a slight decrease at 140 rpm. However, the highest adsorption efficiency of 59.44 % was achieved at 140 rpm. This increase in Fe^{2+} removal at optimal agitation speed is due to the reduction of the film boundary layer surrounding the particles, which enhances the external film transfer coefficient and improves adsorption efficiency [33]. Finally, Figure 4(e) shows the effect of pH on Fe^{2+} removal, adsorption efficiency decreased as the pH increased from 2 to 8, with the highest removal efficiency of 38.01 % observed at 2 pH. This trend is as a result of the competition between metallic ions and hydrogen ions, which influenced the adsorption process [30].

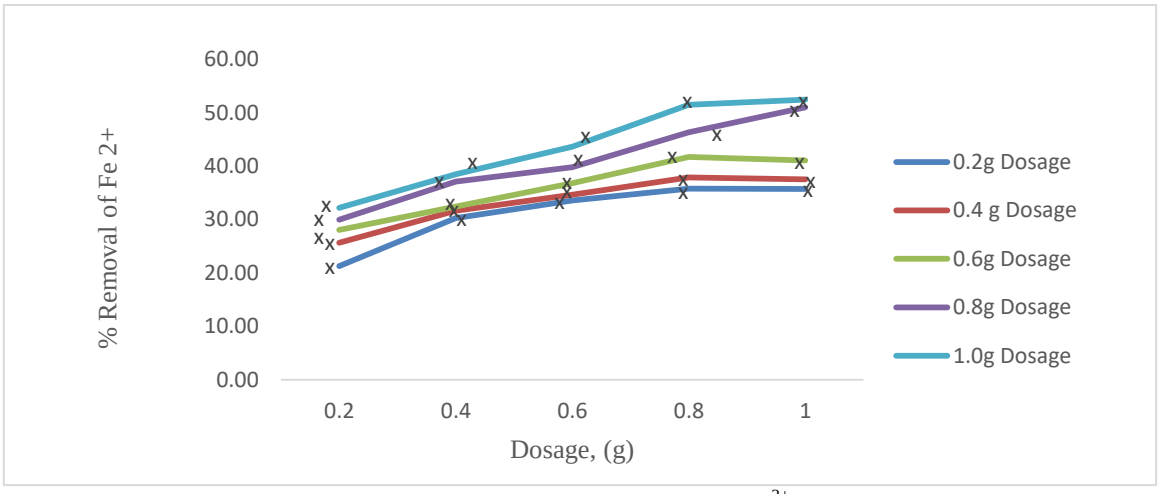

Figure 4 (a): Effect of adsorbent dosage on Fe^{2+} removal

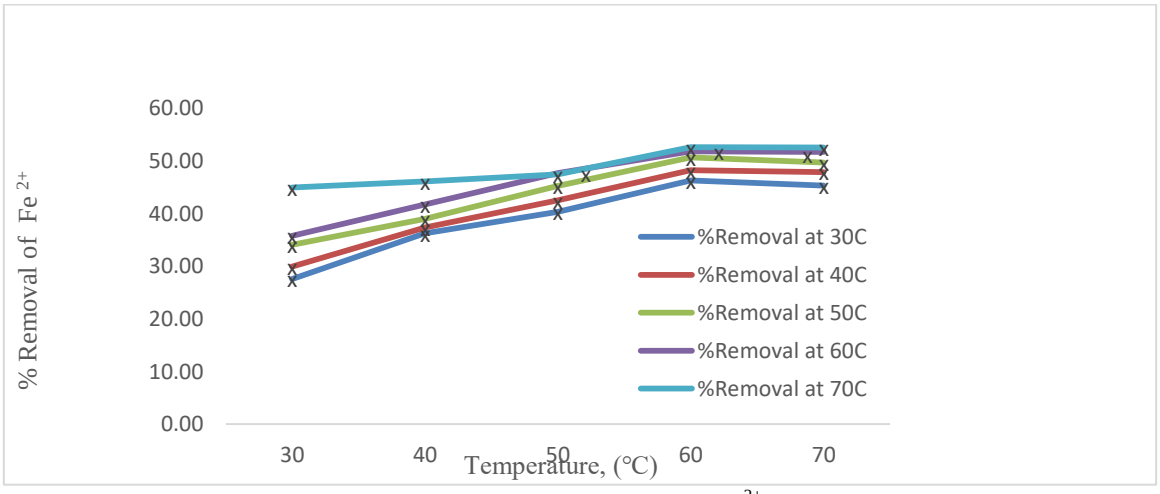

Figure 4 (b): Effect of temperature on Fe^{2+} removal

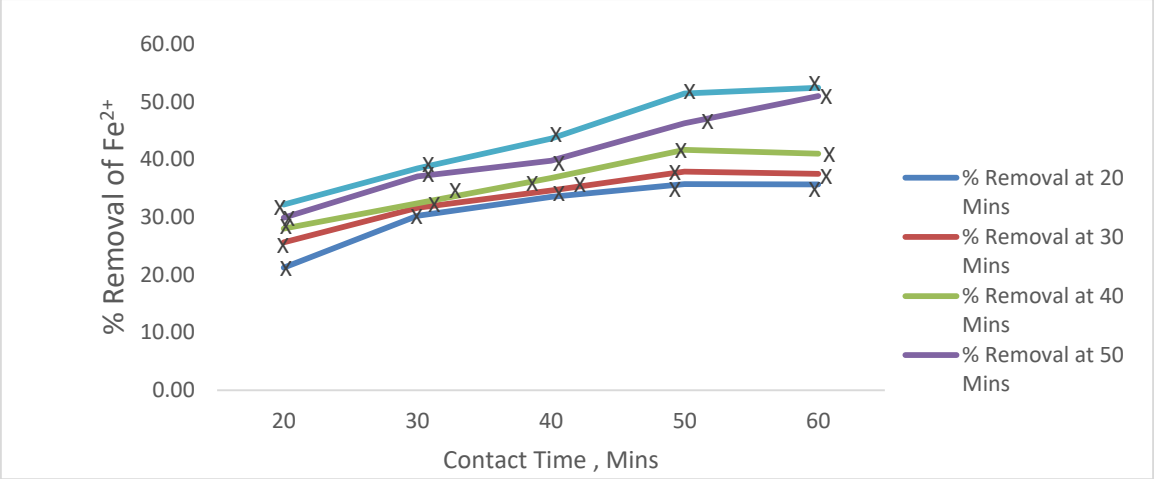

Figure 4 (c): Effect of contact time on Fe^{2+} removal

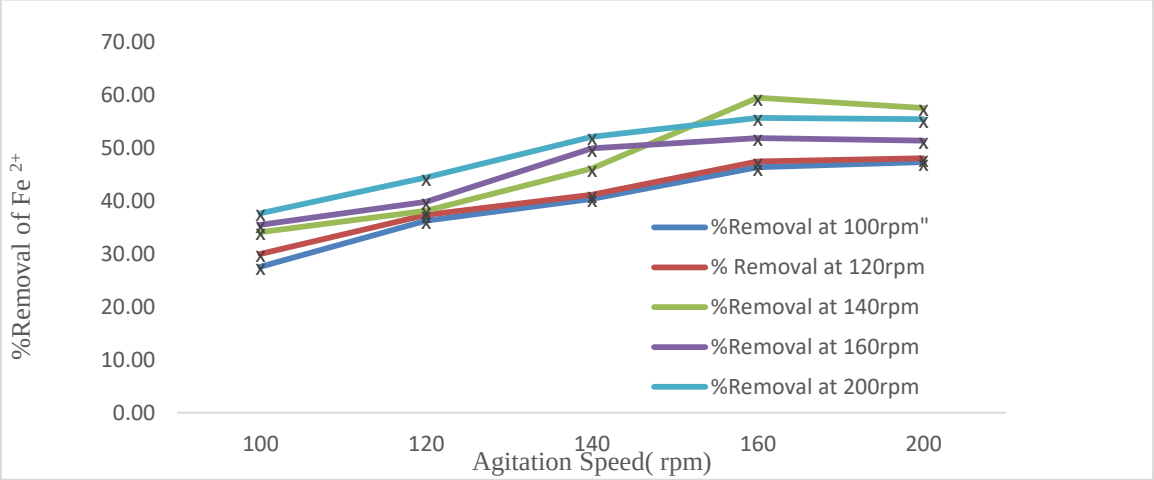

Figure 4 (d): Effect of agitation speed on Fe^{2+} removal

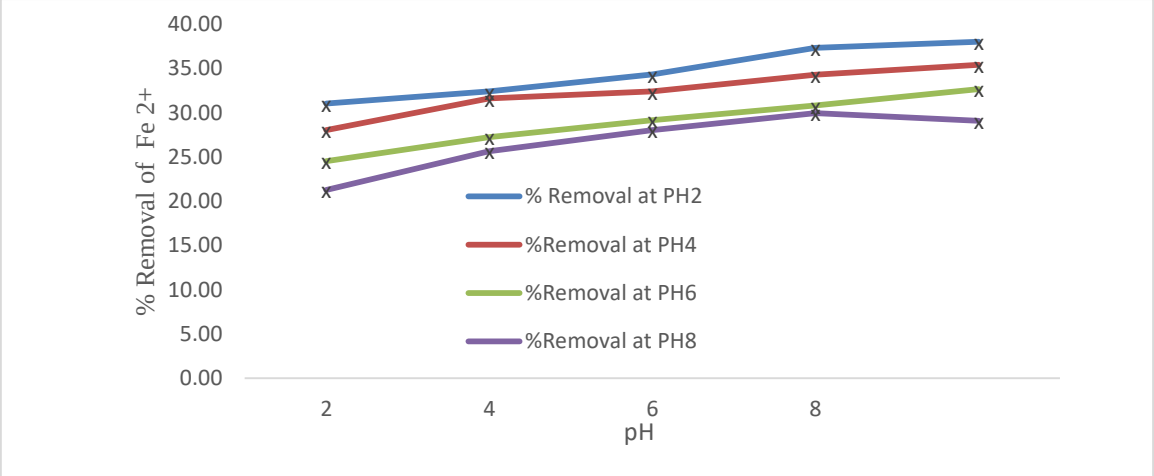

Figure 4 (e): Effect of pH on Fe^{2+} removal

Table 4: Thermodynamics data

30°C				40°C				50°C				60°C				70°C			
Fe Conc. g/l	**qe**	**$K_d=q_e/c_e$**	**ln K_d**	**Fe Conc. g/l**	**qe**	**$K_d=q_e/c_e$**	**lnK_d**	**Fe Conc. g/l**	**q_e**	**$K_d=q_e/c_e$**	**ln K_d**	**Fe Conc. g/l**	**qe**	**$K_d=q_e/c_e$**	**ln K_d**	**Fe Conc. g/l**	**q_e**	**$K_d=q_e/c_e$**	**ln K_d**
0.912	86.75	95.12	4.56	0.88	94.25	106.86	4.67	0.83	107.25	129.22	4.86	0.81	112.5	139.06	4.93	0.69	141.5	204.18	5.32
0.803	57	70.98	4.26	0.79	58.75	74.46	4.31	0.77	61.38	79.92	4.38	0.73	61.38	83.62	4.43	0.68	72.5	106.77	4.67
0.751	42.33	56.37	4.03	0.72	44.58	61.57	4.12	0.69	47.5	68.94	4.23	0.66	47.5	72.08	4.28	0.66	49.75	75.15	4.32
0.676	36.44	53.9	3.99	0.65	37.94	58.19	4.06	0.62	39.88	64.22	4.16	0.61	39.88	65.7	4.19	0.6	41.38	69.31	4.24
0.59	33.45	56.69	4.04	0.58	34.15	59.29	4.08	0.55	35.5	64.66	4.17	0.56	35.5	63.85	4.16	0.54	36	66.79	4.2

Table 5: Thermodynamic parameter for adsorption of Fe^{2+} onto Clay derived Zeolite

TEMP(K)	**ΔS**	**ΔG**	**R^2**
303	37.970038	-11503.8324	0.757
313	38.884578	-12169.6882	0.778
323	40.260545	-13002.8258	0.748
333	41.02959	-13661.3653	0.794
343	44.4799	-15254.3942	0.81

3.5 Thermodynamics Study

The Gibb's free energy, enthalpy, and entropy of adsorption process were determined from the data generated using equations (3) and (4) [34].

$$ln\ K_d = \frac{\Delta H}{R} - \frac{\Delta S}{RT} \quad (3)$$

$$\Delta G = \Delta H - T\Delta S \quad (4)$$

Where, K_d represents dissociation constant, ΔH denotes change in enthalpy, ΔS indicates the change in entropy, ΔG is the change in Gibbs free Energy, R is the universal gas constant, and T represents temperature.

The thermodynamics experimental data for the plot of ln K_d versus 1/T are presented in Table 4 while the R^2 values obtained from the analysis is as shown in Table 5. The slope and intercept provide values of ΔH° and ΔS° respectively, as illustrated in equation 3. The analysis of Gibb's free energy ΔG° shows a negative value for Gibb's free energy across all temperature ranges studied, this depicts that the sorption process is spontaneous in nature and feasible as well [35].

The positive entropy change (ΔS) observed at all temperatures suggests an increase in degree of randomness at the interface between the adsorbate and adsorbent during the adsorption process, highlights the strong affinity of Fe^{2+} ions unto the surface of CDZ. Similarly, the positive values for change in enthalpy were due to endothermic nature of adsorption of Fe^{2+} ions, this can be attributed to the randomness of the process which enhances solid – liquid interaction during the adsorption phenomenon, thereby, facilitating the chemical bonding that took place between the sorbent and sorbate.

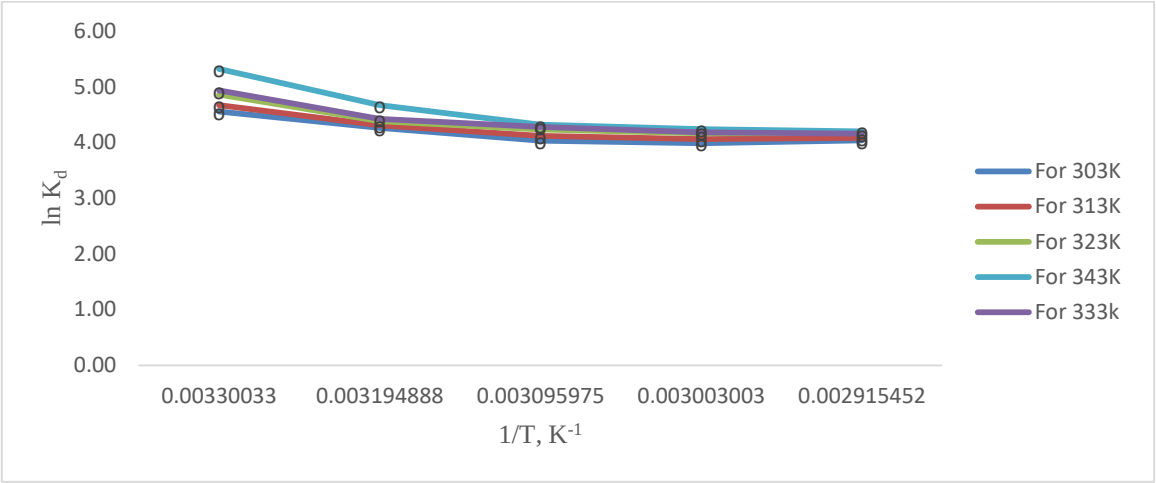

Figure 5: Thermodynamics Graph for the adsorption of Fe^{2+} from produced water using zeolite at different temperatures

4. CONCLUSION

In this study, zeolite was prepared by calcining the clay sample at 600 ℃. After calcination, the sample was dealuminated and synthesized before its application for the adsorption process. Scanning Electron Microscopy (SEM) images reveals the presence of silicate flakes characteristics of kaolinite clay, which contributes to its effectiveness in the adsorption process. Fourier Transform Infra Spectroscopy (FTIR) results reveal the presence of O-H and Si-O functional groups that indicate the adsorptive nature of the clay sample. These functional groups provided surface sites for Fe^{2+} binding. Several parameters investigated such as pH, temperature, contact time, agitation speed, and adsorbent dosage, showed that these parameters significantly influenced the adsorption process. Specifically, an increase in contact time, agitation speed, temperature, and adsorbent dosage enhanced the removal efficiency of Fe^{2+} ions from the produced water. Conversely, as the pH increased from 2 to 8, the sorption rate of Fe^{2+} decreased. Thermodynamics analysis of the adsorption temperature data revealed that the adsorption process was spontaneous, feasible and endothermic.

REFERENCES

[1] Yusrah, H. & Budiyono (2018). Pollution impact and alternative treatment for produced water. *E3S Web of Conference, doi http//doi.org/10.105/e3sconf/20183103004*

[2] EGASPIN (2002). Environmental Guidelines and Standards for the Petroleum Industry in Nigeria Department of Petroleum Resources (Revised) Edition, 80-81.

[3] Chakraborty, R. Asthana, A. K., Singh, B. Jain, & Susan, A. B. H. (2022). Adsorption of heavy metal ions by various low-cost adsorbents: a review. *International Journal of Environmental Analytical Chemistry*, 1-10.

[4] Elham, A. Richard, D. Ashly, E. N. & Kyoungkeun, Y. (2017). Magnetic adsorbents for the recovery of precious metals from leach solutions and wastewater. *Metals*, Vol. 7, No. 12,(1-32)

[5] Wang, S. & Peng. Y. (2010). Natural zeolites as effective adsorbents in water and wastewater treatment. *Chemical Engineering Journal*, 15(6), 11–24.
[6] Zaimee, M.Z.A., Sarjadi, M.S., & Rahman, M.L. (2021). Heavy Metal Removal from Water by Efficient Adsorbents. *Water*, 13(19), 2659.*Doi http://dx.doi.org/10.3390/w13192659*
[7] Tran, H. N., Lima, E. C., Juang, R. S., Bollinger, J. C., & Chao, H. P. (2021). Thermodynamic parameters of liquid–phase adsorption process calculated from different equilibrium constants related to adsorption isotherms: A comparison study. *Journal of Environmental Chemical Engineering*, *9*(6), 106674
[8] Lively, R. P., & Realff, M. J. (2016). On thermodynamic separation efficiency: Adsorption processes. *AIChE Journal*, *62*(10), 3699-3705.
[9] Knight, E. W., Gillespie, A. K., Prosniewski, M. J., Stalla, D., Dohnke, E., Rash, T. A., & Wexler, C. (2020). Determination of the enthalpy of adsorption of hydrogen in activated carbon at room temperature. *international journal of hydrogen energy*, *45*(31), 15541-15552.
[10] Tomul, F., Arslan, Y., Kabak, B., Trak, D., & Tran, H. N. (2021). Adsorption process of naproxen onto peanut shell-derived biosorbent: important role of n–π interaction and van der Waals force. *Journal of Chemical Technology & iotechnology*, *96*(4), 869-880.
[11] Diwald, O., & Hartmann, M. (2021). Adsorption and Chemical Reactivity. *Metal Oxide Nanoparticles: Formation, Functional Properties, and Interfaces*, *2*, 593-636.
[12] Lesne, A. (2014). Shannon entropy: a rigorous notion at the crossroads between probability, information theory, dynamical systems and statistical physics. *Mathematical Structures in Computer Science*, *24*(3), e240311
[13] Du, X., Cheng, Y., Liu, Z., Yin, H., Wu, T., Huo, L., & Shu, C. (2021). CO2 and CH4 adsorption on different rank coals: A thermodynamics study of surface potential, Gibbs free energy change and entropy loss. *Fuel*, *283*, 118886.
[14] Cherkasov, N. (2020). Liquid-phase adsorption: Common problems and how we could do better. *Journal of Molecular Liquids*, *301*, 112378.
[15] Ebelegi, A. N., Ayawei, N., & Wankasi, D. (2020). Interpretation of adsorption thermodynamics and kinetics. *Open Journal of Physical Chemistry*, *10*(3), 166-182.
[16] Barros, L. A., Custodio, R., & Rath, S. (2016). Design of a new molecularly imprinted polymer selective for hydrochlorothiazide based on theoretical predictions using Gibbs free energy. *Journal of the Brazilian Chemical Society*, *27*(12), 2300-2311.
[17] Liu, H., Peng, S., Shu, L., Chen, T., Bao,T. & Frost, R. T. (2013). Effect of Fe_3O_4 addition on removal of ammonium by zeolite NaA. *Journal of Colloid and Interface Science,* 390 (1), 204–210.
[18] Olaremu, A.G. (2015). Sequential Leaching for the Production of Alumina from a Nigerian Clay" International Journal of Engineering Technology, Management and Applied Sciences, Volume 3, Issue 7,103-109.
[19] Tegin, I. & Saka, C. (2021). Chemical and thermal activation of clay sample for improvement adsorption capacity of methylene blue. *International Journal of Environmental Analytical Chemistry.*, 103(16): 1-12. Doi: 10.1080/03067319.2021.1928105.
[20] Ajayi, O., Atta, A., Aderemi., & Adefilla, S.S. (2010). Novel method of metakaolin dealumination –preliminary investigation. Journal of Applied Science Research. 6(10): 1539-1546.
[21] Pandiangan, K., Simanjuntak, W., Pratiwi, E. & Rilyanti, M.m (2019). Characteristics and catalytic activity of zeolite- a synthesized from rice husk silica and aluminum metal by sol-gel method. *Journal of Physics Conference Series*. 1338(1): 012015 DOI 10.1088/1742-6596/1338/1/012015
[22] American Public Health Association (APHA) (2005). Standard Methods for the examination of water and wastewater. USA: *American Public Health Association* (APHA).
[23] Yousef, R., Qiblawey, H.,El-Naas, M.H.(2020). Adsorption as a Process for Produced water Treatment: A Review. Wastewater Treatment Processes 8(12), 1657
[24] Isehunwa, S.O & Onovea, S. (2011). Evaluation of Produced water discharged in the Niger-Delta. APRN Journal of Engineering and Applied Sciences 6(8), 66-72.
[25] Nayak, P.S & Singh, B.K. (2007). Instrumental characterization of clay by XRF, XRD and FTIR *Bull. Mater. Sci.*, Vol. 30, pp. 235–238. http://doi.org/10.1007/s12034-007-0042-5
[26] Jozanikohan, G., & Abarghooei, M.N. (2022). The Fourier transform infrared spectroscopy (FTIR) analysis for the clay mineralogy studies in a clastic reservoir. *J Petrol Explor Prod Technol* Vol.12 2093-2106 https://doi.org/10.1007/s13202-021-01449-y
[27] FTIR Functional Group Database Table with Search-InstaNANO. http://instanano.com/all/characterization/ftir/ftir-functional-group-search / (accessed January 13th 2025)
[28] Ihekweme G.O, Shondo J.N, Orisekeh K. I, Onwualu P.A, Kalu-uka G.M. & Nwuzor, I.C (2020) Characteristics of certain Nigerian clay minerals for water purification and other industrial application, Heliyon*: e03783*
[29] Ural, N.(2021). The significance of scanning electron microscopy(SEM) analysis on the microstructure of improved clay: An overview. Open Geosciences, 13(1), 197-218. Doi http://doi.org/10.1515/geo-2020-0145
[30] Wang, S., Li, L. & Zhu, Z. H. (2007). Solid-state conversion of fly ash to effective adsorbent for Cu removal from wastewater, *J. Hazard Mater.*, 139, 254-259

[31] Kubilay, S., Gurkan, R., Savaran, A., & Sahan, A. (2007). Removal of Cu (II), Zn ((II) and Co (II) ions from aqueous solution by adsorption onto natural bentonite. Adsorption 13: 41-5. http: //dx.doi.org/10.1016/j.colsurfa.2009.06.036.
[32] Javadian, H., Ghorbani, F., Tayebi, H.A. and Asl, S. H. (2015). Study of the adsorption of Cd(II) from aqueous solution using zeolite- based geopolymer, synthesized from coal fly ash; kinetic, isotherm and thermodynamics studies. *Arabian Journal of Chemistry*, 8, 837-849.
[33] Ali, A. A., Elasala, G. S., Elmeleigy, E.M. & Saeed, A.R. (2021). Adsorption of Cu (II) ions from aqueous solutions using low cost material. Chemistry Research Journal. 6(4): 31-48
[34] Mandal, A., Mukhopadhyay, P.& Das, S.K. (2019). The Study of adsorption efficiency of rice husk ash for the removal of phenol from wastewater with low initial phenol concentration. *SNAppl.sci. 1, 192.* *https://doi.org/10.1007/s42452-019-0203-3*.
[35] Singha, B. & Das, S. K. (2011). Biosorption of Cr (VI) ions from aqueous solutions: Kinetics, equilibrium, thermodynamics and desorption studies. *Biointerfaces*, vol. 84 (1), 221–232.